Apelin-13 in the paraventricular nucleus (PVN) attenuates myocardial ischemia through V1a receptors in PVN/nucleus tractus solitarii (NTS) and GARγ2 in NTS

WEN YAN[1], DAN WANG[2], XINMIN ZHANG[2] and CHENGLUAN XUAN[2]

[1]Department of Anesthesia, The Second Hospital of Jilin University, Changchun, Jilin 130021, P.R. China;
[2]Department of Anesthesia, The First Hospital of Jilin University, Changchun, Jilin 130021, P.R. China

Received June 26, 2025; Accepted September 4, 2025

DOI: 10.3892/ijmm.2025.5652

Abstract. The apelin system plays a significant role in central blood pressure regulation, but its role in the neural control of myocardial protection remains poorly understood. The present study evaluated the effects of apelin-13 in the paraventricular nucleus (PVN) on myocardial infarction (MI). In a male rat MI model, apelin-13 expression was decreased in PVN, while Vasopressin 1a (V1a) receptor expression was increased in both PVN and nucleus tractus solitarii (NTS) and $GABA_A$ receptor (GAR)γ2 expression was increased in NTS. Cardiac function was assessed after microinjection of apelin-13 or gene transfer of apelin-13 into the PVN. Apelin-13 overexpression in PVN markedly improved MI cardiac function, as evidenced by left ventricular end-diastolic diameter, left ventricular end-systolic diameter, left ventricular ejection fraction and left ventricular fractional shortening, along with decreased plasma noradrenaline and increased vasopressin levels. Mechanistically, both TGF-β/Smad signaling and Bax/Bcl-2 expression were implicated in heart tissue. Additionally, serum levels of four parasympathetic neuropeptides (somatostatin, cholecystokinin, glucagon-like peptide-1 and vasoactive intestinal peptide) were elevated in parallel with cardiac function improvement. Notably, V1a receptor antagonist administration in PVN/NTS or GAR agonist treatment in NTS attenuated the cardioprotective effects of apelin-13. These findings demonstrated that PVN apelin-13 overexpression improves cardiac function through V1a receptors (PVN/NTS) and GARγ2 (NTS), involving both parasympathetic neuroendocrine activation and modulation of myocardial apoptotic/inflammatory pathways. The present study provided novel insights into neural mechanisms of cardiovascular regulation.

Correspondence to: Dr Chengluan Xuan, Department of Anesthesia, The First Hospital of Jilin University, 1 Xinmin Street, Changchun, Jilin 130021, P.R. China
E-mail: xuancl@jlu.edu.cn

Key words: apelin-13, paraventricular nucleus, nucleus tractus solitarii, myocardial protection

Introduction

Brain-heart crosstalk is now referred to as neurocardiology, which addresses the effects of brain injury on the heart or the effects of cardiac injury on the brain (1). There is increasing experimental and clinical evidence not only suggesting a causal link from the heart to the brain but also indicating the presence of a bidirectional relationship, highlighting the powerful influence of the brain on the heart (2).

Hypothalamus-pituitary-adrenal (HPA) axis activation plays a pivotal role in communication between the brain and heart, leading to cardiac dysfunction (3). As the primary integrator of this axis, the paraventricular nucleus (PVN) of the hypothalamus acts as the primary integrator that modulates HPA axis activity, which can increase blood pressure, alter heart rate and promote inflammation in the cardiovascular system (4). The PVN is also a master controller of the autonomic nervous system, which provides specialized innervation to all autonomic relay centers (5), projecting to the rostral ventrolateral medulla (RVLM) and spinal cord to regulate sympathetic outflow (6). Notably, a reduction in PVN activity promotes the improved recovery of cardiac function after myocardial infarction (6).

Apelin, containing 77 amino acids, has been isolated from bovine stomach extracts and its effects are mediated via ligands for the orphan G-protein-coupled (APJ) receptor (7,8). Apelin-13 is the main isoform that activates the APJ receptor. As a novel regulator of activity, the apelin/APJ system is involved in neurohumoral regulation of the HPA (9) and emerging evidence indicates that apelin-13 and the APJ receptor are widely expressed in microglia and neurons of the central nervous system (CNS) (10). Microinjection of apelin-13 into the PVN increases c-Fos-like immunoreactivity in the PVN after 1.5 h (11), while chronic infusion of apelin-13 in the PVN induces long-term hypertension and sympathetic activation mediated by superoxide anions (12). Based on previous data, apelin-13 may affect the cardiovascular system via the vasopressinergic system in the PVN and supraoptic nucleus of the hypothalamus (13-15). A reduction in APJ mRNA expression has been observed in the hypothalamus in postinfarct heart failure, especially in presynaptic neurons of the PVN, which could attenuate the pressor response to intracerebroventricularly infused apelin-13 (16).

γ-Aminobutyric acid (GABA) is a well-known neuronal transmitter that exerts inhibitory effects on the brain via the $GABA_A$ receptor (GAR) and $GABA_B$ receptor (GBR), which have been defined on the basis of pharmacological and physiological research (17). According to our previous study, the GABAergic system in the medullary nucleus tractus solitarii (NTS) contributes to the central resetting of blood pressure and the development of hypertension (18). NTS is reciprocally connected with the pontine parabrachial and Kölliker-Fuse nuclei to relay visceral afferent information to other central autonomic network structures (19). Baroreceptor activation inhibits vasopressin secretion, which might be regulated by the activation of GABAergic projections to vasopressinergic neurons and the local administration of a GAR antagonist inhibits vasopressinergic neurons during the onset of hypertension (20). Thus, the apelin/APJ system, vasopressinergic system and GABAergic system are vital pathways of the CNS involved in the neural control of the cardiovascular system in the hypothalamus, but they remain poorly understood in relation to myocardial injury.

The parasympathetic endocrine system (PES) comprises circulating peptides released from secretory cells that are markedly modulated by vagal projections from the dorsal motor nucleus of the vagus nerve (21). A total of four peptides present in the circulatory system, isomatostatin (SST), cholecystokinin (CCK), glucagon-like peptide 1 (GLP-1) and vasoactive intestinal peptide (VIP), perform sympathetic antagonism to balance sympathetic activation-induced pupillary dilation and increase the rate and contractility of the heart (22).

The present study aimed to assess the effects of apelin-13 in the PVN on the cardiac function of rats with myocardial infarction (MI). The involved mechanisms, including myocardial ischemia-related apoptotic and inflammatory pathway markers in the heart and neuropeptides in the serum, were also explored.

Materials and methods

All animal procedures were conducted in accordance with the institutional guidelines of The First Hospital of Jilin University and were approved by the Institutional Animal Care and Use Committee (approval no. 2020-0128). All studies were approved locally and conformed to the guidelines from Directive 2010/63/EU of the European Parliament on the protection of animals used for scientific purposes. The male Sprague-Dawley rats were purchased from Charles River. A total of 246 male rats were used in the present study (250-300 g; age, 8 weeks). The rats were maintained under a 12-h light/dark cycle at a temperature of 20±2˚C and a relative humidity of 55±5%. Food and water were provided *ad libitum*. The rat studies were performed under isoflurane anesthesia (2.0-2.5% isoflurane, 100% oxygen at 2 l/min) in spontaneous breathing. To perform histology studies and blood tests, sodium pentobarbital (40-60 mg/kg) was intraperitoneally injected to anesthetize the rats. The present study typically used an initial dose of 40 mg/kg and occasionally administered additional doses based on the condition of the rat. The rats were then sacrificed by exsanguination while still under anesthesia. Explanations of each reagent and buffer are presented in Appendix S1, Tables SI and SII.

Myocardial infarction (MI). Male SD rats at 8 weeks of age were randomly selected for MI modelling via left anterior descending (LAD) artery ligation. Anesthesia was induced and maintained in the SD rats with isoflurane (1-2% oxygen). Following anesthesia, the animals were intubated and ventilated with a 16-gauge intravenous catheter and placed in a supine position on a temperature control pad. Left-sided thoracotomy was performed via a small incision between the third and fourth intercostal spaces. The incision was expanded by a blunt-ended retractor such that the lungs were not retracted. The pericardial sac surrounding the heart was cut open to access the heart. The heart was not exteriorized. Using a tapered atraumatic needle, a 5-0 silk Prolene suture ligature was passed underneath the LAD and tied with three knots. Visible blanching and cyanosis of the anterior wall of the left ventricle and swelling of the left atrium were indicative of successful ligation. Rats subjected to cardiac exposure without coronary ligation served as the sham-operated control group.

Western blot analysis. Micropunched NTS or PVN tissue from the brain sections of the rats was treated with 1 ml lysis buffer, homogenized for 15 sec, boiled for 3 min, ultrasonicated and centrifuged. The supernatants were stored in a -80˚C freezer.

Vasopressin 1a (V1a) receptor protein levels in neuronal cultures were assessed using western blot analysis. Cultures were washed with ice-cold PBS, scraped into lysis buffer containing 8 μl/ml inhibitor cocktail and centrifuged at 10,000 x g for 10 min at 4˚C. The supernatant was saved for the protein assay.

Murine heart lysates were prepared by digesting tissues in lysis buffer with protease and phosphatase inhibitors and PMSF using a Qiagen Tissue Lyser (Qiagen GmbH; 50 rpm; 8 min; 4˚C), followed by rocking for 1 h at 4˚C, sonication on ice using 20 kHz in a pulse mode (3 sec on/5 sec off) for 10 cycles and centrifugation at 12,000 x g for 20 min at 4˚C, with supernatants stored at -80˚C.

The protein concentration was determined with a BCA protein concentration assay kit. For each sample, 20 μg protein was separated on a 10% SDS-PAGE gel and transferred to nitrocellulose membranes (100 V, 2 h). Membranes were blocked in PBS-T containing 10% milk and 1% bovine serum albumin (BSA) for 3 h, then incubated overnight at 4˚C with primary antibodies (anti-apelin polyclonal antibody, anti-GAR γ2 antibody, anti-$GABA_B$ receptor1 antibody, anti-V1a receptor antibody, anti-TGF-β1 antibody, anti-Smad2 antibody, anti-Bax antibody and anti-Bcl-2 antibody; Table SI). After washing (15 min PBS-T with 0.1% Tween followed by four 5-min PBS-T washes), the membranes were incubated for 2 h at room temperature in horseradish peroxidase-conjugated anti-rabbit or anti-mouse antibodies diluted 1:5,000. Immunoreactivity was detected by enhanced chemiluminescence (Beyotime Institute of Biotechnology) and the protein bands were analyzed with ImageJ (National Institutes of Health; v.1.53q).

Reverse transcription-quantitative (RT-q) PCR. The present study used RT-qPCR to detect changes in the expression of apelin-13, V1a receptor, GBR1 and GARγ2 in the PVN and NTS of the rats and in the neuronal cultures. The isolation of total RNA from PVN and NTS tissue and neuronal cultures was performed with a RNeasy Mini Kit (cat. no. 74104; Qiagen

GmbH) in accordance with the manufacturer's instructions. RNA purity and concentration were determined spectrophotometrically (Nanodrop 2000c; Thermo Fisher Scientific, Inc.). For each RT-qPCR, 2 μg of total RNA was converted into cDNA with reverse transcriptase. Genomic DNA was eliminated by DNase I. Real-time PCRs were performed in a 10 μl total reaction volume using 96-well plates with the QuantiTect SYBR Green PCR Kit (cat. no. 208054; Qiagen GmbH) and the relative difference was expressed as the fold change compared with control values, calculated using the comparative cycle method (23). The RT-qPCR system (ABI 7500; Applied Biosystems; Thermo Fisher Scientific, Inc.) with the following protocol: Initial denaturation at 95˚C for 30 sec, followed by 40 cycles of 95˚C for 5 sec and 60˚C for 34 sec. All steps adhered to the manufacturers' protocols and each condition was assayed in three technical replicates. Data were normalized to 18S rRNA. The sequences of the primers are presented in Table SIII.

Brain nucleus microinjection. The rats were anaesthetized with a mixture of oxygen and isoflurane (2-2.5%) via a nose cone. They were placed in a stereotaxic frame (DW-2000, Chengdu Techman Co., Ltd.). The skin overlying the midline of the skull was incised and a small hole was drilled bilaterally on the dorsal surface of the cranium according to the nucleus coordinates (24), including the PVN (bregma -1.92 mm, interaural 7.08 mm, midline 0.5, 5.8 mm ventral to the dura mater) and NTS (bregma -13.68 mm, interaural -4.68 mm, midline 0.5, 8.0 mm ventral to the dura mater). A microsyringe was positioned in the nucleus and controlled by a microsyringe pump controller.

i) Apelin gene transfer: The AAV2-apelin-13 virus or AAV2-GFP ($5x10^{12}$ GC/ml in 50 nl) was microinjected unilaterally (right) into the PVN to induce endogenous apelin expression.

ii) Osmotic mini-pump implantation: A 28-gauge lower end of a stainless-steel cannula (Alzet Brain Infusion Kit 2; Durect Corporation) was implanted into the right NTS or PVN according to the nucleus location aforementioned and then fixed on the skull with dental cement. The upper end was connected to an osmotic mini-pump for chronic continuous intranuclear infusion at 0.11 μl/h for 4 weeks. The pumps were filled with apelin-13 (100 μM; 100 μl) (25,13), a GAR agonist (muscimol; 100 μM, 100 μl) (18), or a V1a receptor antagonist (SR49059; 200 μM, 100 μl) (26) and placed subcutaneously on the backs of the rats.

Echocardiography. Echocardiography was performed under inhaled anesthesia with isoflurane (1-2% oxygen) using a 14-MHz transducer at a depth of 1 cm for two-dimensional imaging. M-mode images were taken at the mid-papillary muscle level and were used for measurements.

Blood sample tests. Blood collected in a serum separation tube was allowed to clot at room temperature for 30 min before being centrifuged at 1,000 x g for 15 min. The serum from each subject was either used immediately for analysis or divided into aliquots and stored at -20˚C for future use. The levels of somatostatin, cholecystokinin, glucagon-like peptide-1 and vasoactive intestinal peptide in the serum were quantified using enzyme-linked immunosorbent assay (ELISA) kits: Somatostatin (cat. no. NBP2-80271; Novus Biologicals; Bio-Techne), cholecystokinin (cat. no. EIAR-CCK-1; RayBiotech, Inc.), glucagon-like peptide-1 (cat. no. E-EL-R3007-96T; Wuhan Elabscience Biotechnology Co., Ltd. Wuhan Elabscience Biotechnology Co., Ltd.), and vasoactive intestinal peptide (cat. no. NBP2-82466; Novus Biologicals; Bio-Techne). A commercial arg^8-Vasopressin ELISA kit (cat. no. ADI-900-017A; Enzo Life Sciences) and a noradrenaline competitive ELISA kit (cat. no. EEL010; Thermo Fisher Scientific, Inc.) were used for the quantitative measurement of plasma vasopressin and noradrenaline levels.

Cardiac immunohistochemistry and multiplex fluorescent immunohistochemistry staining. To assess the alterations in TGF-β1, Smad2, Bax and Bcl-2 expression in cardiac tissues, the heart samples were fixed in 4% paraformaldehyde at 4˚C for 24 h and embedded in paraffin. Briefly, tissues were dehydrated in graded ethanol (70-100%), cleared in xylene, infiltrated with paraffin wax at 60˚C and embedded in molds for solidification. All steps were performed with agitation. To perform immunohistochemical staining, samples were sectioned at 4-5 μm thickness. Following deparaffinization and rehydration, antigen retrieval was conducted using citrate buffer (pH 6.0) at 95˚C for 20 min. After blocking endogenous peroxidase activity with 3% H_2O_2 and nonspecific binding sites with normal serum (cat. no. abs933; Absin), sections were incubated with primary antibodies (TGF-β1, Smad2, Bax and Bcl-2) overnight at 4˚C. HRP-conjugated secondary antibodies were then applied, followed by DAB development (room temperature; 10 min) and hematoxylin counterstaining (room temperature; 5 min). Finally, sections were dehydrated, cleared in xylene and mounted for microscopic examination. The multiplex fluorescent immunohistochemistry staining was performed on 4-μm paraffin-embedded cardiac sections using sequential tyramide signal amplification. Following deparaffinization and initial antigen retrieval in citrate buffer (pH 6.0), sections were blocked and incubated with the first primary antibody at 4˚C 16 h, followed by HRP-conjugated secondary antibody and TSA570 development. Following microwave stripping in citrate buffer, the cycle was repeated for Bax, SMAD2 and Bcl-2, with sodium azide treatment between each round to inactivate residual HRP activity. Nuclei were counterstained with DAPI (room temperature; 5 min) and slides were mounted with anti-fade medium. Multispectral imaging was performed using a Vectra system (AKOYA Vectra Polaris; AKOYA Inform 2.6; Akoya Biosciences, Inc.), with spectral unmixing to separate fluorophore signals.

Rat apelin-13 gene adeno-associated virus type 2 (AAV2) production. The rat apelin-13 gene was synthesized by Wuhan Beisai Model Biotechnology Co., Ltd. The CMV promoter partial sequence and the mCherry partial sequence were connected to both ends of the gene (Appendix S1). The virus concentration was $5x10^{12}$ GC/ml. The information concerning the apelin-13 gene from NCBI is described in Appendix S1.

Primary neuron culture. Primary neuron cultures were prepared from brain of 1-day-old neonatal rats. The neonatal

rats were euthanized via an intraperitoneal injection of sodium pentobarbital at a dose of 150 mg/kg and washed with 70% ethanol. Brain tissue (from 5-7 rats) was mechanically dissociated in Solution D by pipetting 10 times. Cells were further dissociated with 0.25% trypsin and DNase I (496 U/ml), resuspended in DMEM containing 10% PDHS and plated onto poly-L-lysine-precoated (for at least 4 h) Nunc plastic tissue culture dishes. Prior to plating, the cell suspension was diluted to the required number of cells/unit volume ($3x10^6$ cells/2 ml) of medium per 35-mm dish. The cells were grown in a humidified atmosphere with 95% O_2 and 5% CO_2 for 3 days, after which the culture medium was replaced with fresh DMEM containing cytosine arabinoside (ARC; 1 μM) and 10% PDHS. After 3 days, the ARC was removed and replaced with normal medium for an additional 5-9 days before use.

Immunocytochemistry of neuronal cultures. Neuronal cultures from newborn Sprague-Dawley rats were washed briefly with Dulbecco's PBS three times and then fixed with PBS containing 0.1% Tween 20 (PBS/Tween) and 4% formaldehyde solution for 15 min at 4˚C. After three brief PBS-Tween washes, cells were blocked with 10% goat serum in PBS-Tween at 37˚C for 30 min. The blocking solution was completely removed without additional washing. Primary antibodies (rabbit anti-rat APJ or V1a antibody) diluted in 1 ml PBS-Tween were added and incubated at 4˚C overnight. Following three 3-min PBS-Tween washes, neurons were incubated with appropriate secondary antibodies for 1 h (Alexa Fluor 488-conjugated goat anti-rabbit IgG; cat. no. 4412S; CST; 1:1,000) and washed three times (3 min each) with PBS-Tween. Nuclei were stained with DAPI at room temperature for 5 min, washed four times thoroughly, then mounted with anti-fade medium under glass coverslips.

Masson's trichrome staining. To evaluate cardiac morphological changes and the extent of cardiac fibrosis, heart tissues were fixed in 4% paraformaldehyde for 24 h and embedded in paraffin. Cardiac fibrosis was determined using Masson's trichrome staining of 4%-PFA-fixed, paraffin-embedded, 4-μm-thick heart cross-sections. Briefly, dewaxed sections are treated with potassium dichromate overnight, rinsed, then stained with Ponceau S (5-10 min). After washing, slides are treated with phosphomolybdic acid (1-3 min), directly stained with aniline blue (30 sec-2 min), and differentiated in 1% acetic acid. Images were captured by light microscopy for analysis. The fibrotic fraction was obtained by calculating the ratio of blue (fibrotic) to total myocardial area using ImageJ (v.1.53q; National Institutes of Health).

TUNEL staining. For apoptosis and α-actin co-staining, formalin-fixed, paraffin-embedded heart sections were first deparaffinized. Antigen retrieval was performed using the steamer method in citric acid antigen repair buffer (pH 6.0), followed by blocking with 3% goat serum at room temperature for 30 min. The sections were incubated with terminal deoxyribonucleotidyl transferase (TdT) mixed with deoxyuridine triphosphate (dUTP; 1:10) at 4˚C overnight. The following day, the sections were washed with PBS three times and then nuclei were stained with DAPI for 10 min at room temperature. After three washes with PBS, the sections were mounted with an anti-fade mounting medium.

Triphenyltetrazolium chloride (TTC) staining. After anaesthetizing the rats, heart tissue was collected immediately and cold PBS was used to perfuse the left ventricle within 5 min. The heart was then stored at -20˚C for 20-30 min. Each heart was sectioned into five 2-mm transverse slices, which were stained with preheated TTC solution for 15-30 min at 37˚C. Next, the sections were fixed in 4% formaldehyde (room temperature; 24 h) and images of the TTC-stained sections were captured. The cardiac infarction area was pale and normal cardiac tissue was red. The infarct size was quantified as the total infarct area divided by the area at risk using ImageJ ((v.1.53q; National Institutes of Health).

Statistical analysis. The number of samples (n) used in each experiment is indicated in the legends or shown in the figures and indicates biological replicates. The results are presented as the mean ± standard deviation (SD) or standard error of the mean (SEM). The normality of the data was assessed using the Shapiro-Wilk test. For datasets with a normal distribution, statistical analyses were performed via an unpaired two-tailed t test or one-way analysis of variance (ANOVA) with Tukey's multiple-comparisons test and Dunnett's multiple-comparisons test. Two groups were statistically compared via the unpaired Mann-Whitney U test if the datasets did not pass the normality test. Statistical analyses were performed using PRISM (GraphPad Software Inc.; Dotmatics; version 10). Post-hoc power analysis was conducted for all key statistical comparisons using the observed effect sizes and variances via the WebPower platform (webpower.psychstat.org). $P<0.05$ was considered to indicate a statistically significant difference.

Results

Expression of apelin-13, the V1a receptor and the GARγ2 receptor in MI model rats. On day 28 following MI, apelin-13 expression was markedly lower at both the protein and mRNA levels in the PVN but not in the NTS or RVLM in MI model rats compared with sham rats (Fig. 1A-C). V1a receptor expression was increased in the PVN and NTS but not in the RVLM at both the protein and mRNA levels (Fig. 1A, D and E). GARγ2 was higher in the NTS but not in the PVN or RVLM in MI model rats compared with sham control rats (Fig. 1A, H and I). By contrast, GBR1 expression was not markedly affected (Fig. 1A, F and G). These findings indicated that apelin-13 expression was downregulated in the PVN of MI rats and suggested that both V1a receptors and GARγ2 may play a role in central nervous system regulation of MI within the PVN and nucleus NTS.

Effects of apelin-13 microinjection into the PVN on cardiac function in MI model rats. The present study investigated the effects of continuous exogenous apelin-13 infusion into the PVN on MI rats using osmotic minipump implantation. MI models were established one day after implanting an osmotic mini-pump with apelin-13 into the PVN (Fig. 2A). Continuous apelin-13 infusion into the PVN of MI rats increased V1a receptor expression in the PVN and NTS but decreased GARγ2 expression in the NTS (Fig. 2B-D). Echocardiography on day 28 after MI revealed improved cardiac function in the rats that received continuous apelin-13 infusion into the

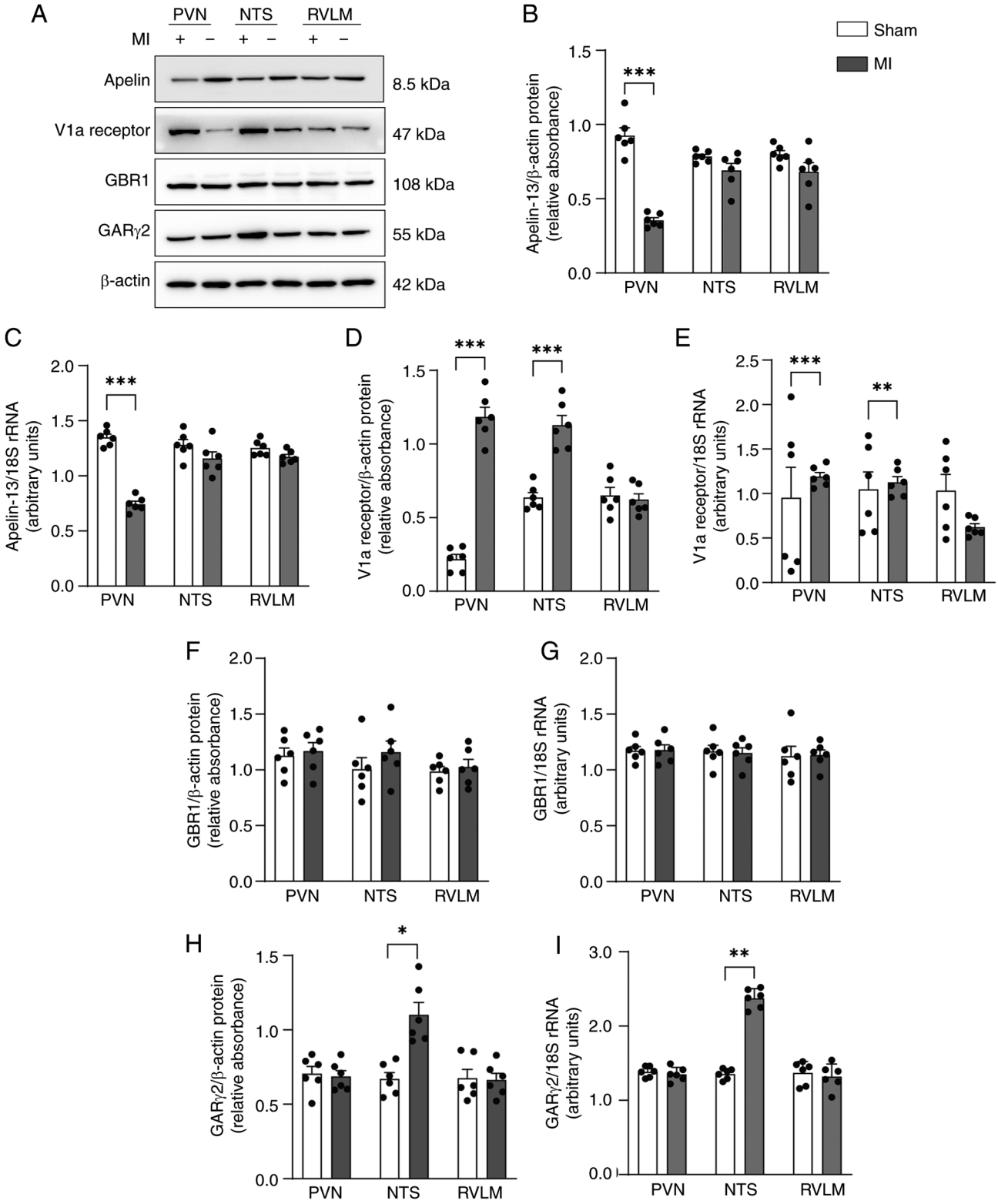

Figure 1. Expression of apelin-13, the V1a receptor and the GARγ2 receptor in MI model rats. (A) Representative western blots of apelin-13, the V1a receptor, the GBR1 and the GARγ2 in the PVN, NTS and RVLM from MI model rats and sham-operated control rats. (B) Quantification of apelin-13 protein levels. (C) mRNA expression levels of apelin-13. (D) Quantification of V1a receptor protein levels. (E) mRNA expression levels of the V1a receptor. (F) Quantification of GBR1 protein levels. (G) mRNA expression levels of GBR1. (H) Quantification of GARγ2 protein levels. (I) mRNA expression levels of GARγ2. Normality was tested using the Shapiro-Wilk test. The data (n=6 rats per group; 3 technical replicates) in B-I are shown as mean ± SEM and were analyzed using an unpaired two-tailed t test. *P<0.05; **P<0.01; ***P<0.001. Post-hoc power exceeded 80% for all comparisons. V1a, Vasopressin 1a; GAR, $GABA_A$ receptor; MI, myocardial infarction; GBR1, $GABA_B$ receptor1; PVN, paraventricular nucleus; NTS, nucleus tractus solitarii; RVLM, rostral ventrolateral medulla.

PVN (Fig. 2E). Specifically, these rats presented a greater lower left ventricular end-diastolic diameter (LVEDD; 6.34±0.45 vs. 8.06±0.16 mm, P<0.01; Fig. 2F), lower left ventricular end-systolic diameter (LVESD; 5.97±0.20 mm

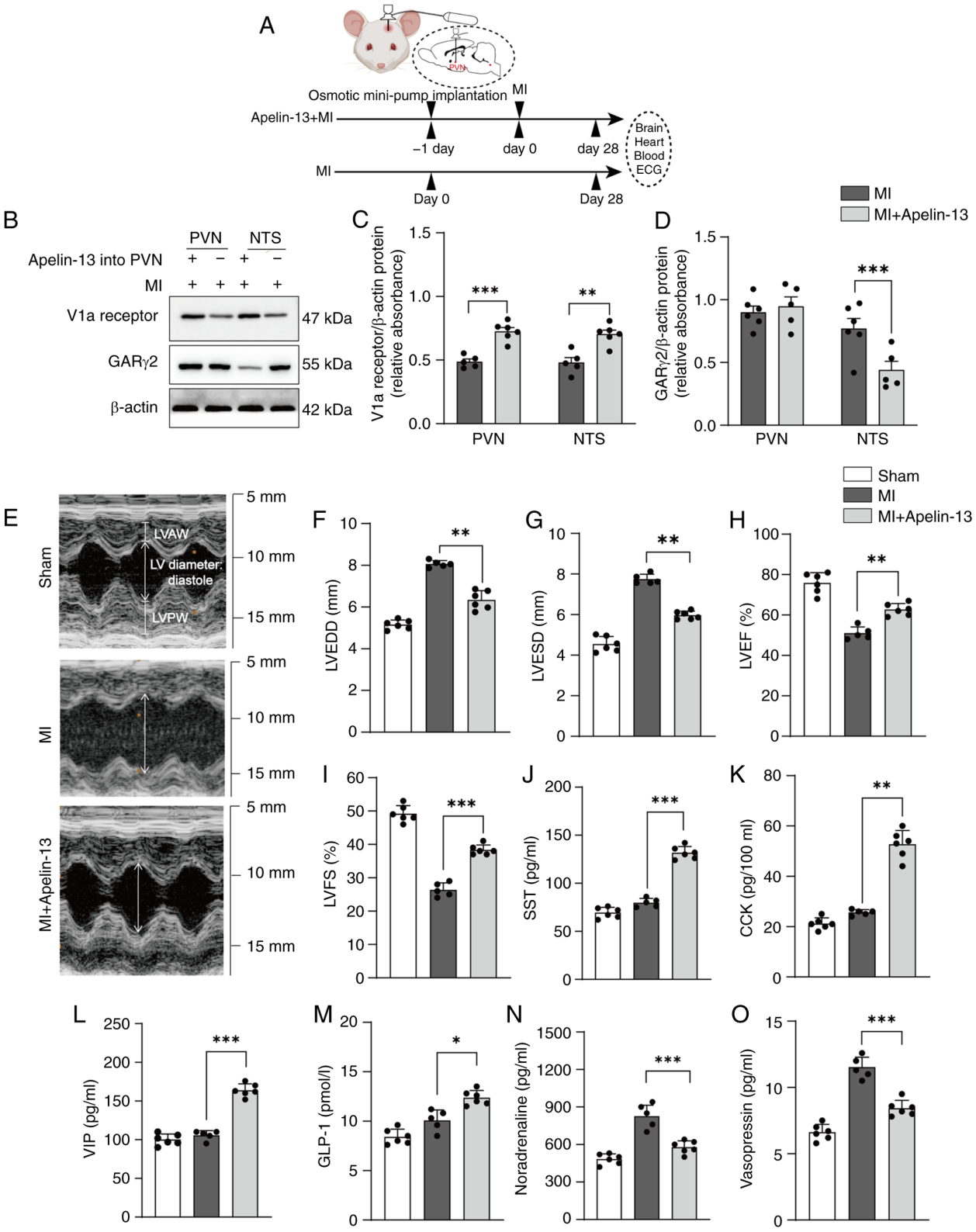

Figure 2. Effects of apelin-13 microinjection into the PVN on cardiac function in MI model rats. (A) MI models were established one day after implanting an osmotic mini-pump delivering apelin-13 into the PVN. Cardiac function was assessed and tissue samples were collected 28 days after mini-pump implantation. (B) Representative western blots for the V1a receptor and GARγ2 in the PVN and NTS from MI model rats and MI model rats continuously microinjected with apelin-13 into the PVN for 28 days. (C) Quantification of V1a receptor protein levels. (D) Quantification of GARγ2 receptor protein levels. (E) Representative ultrasound images (M-mode) performed on days 28 after MI and sham-operated control. Echocardiographic results for (F) LVEDD, (G) LVESD, (H) LVEF and (I) LVFS (n=6 in the sham-operated control group; n=5 in the MI group, one rat succumbed at 20 days; n=6 in the MI + apelin group). Plasma levels of (J) SST, (K) CCK, (L) VIP, (M) GLP-1, (N) noradrenaline and (O) vasopressin (n=6 in the sham-operated control group; n=5 in the MI group, one rat succumbed at 20 days; n=6 in the MI + apelin group). Normality was tested using the Shapiro-Wilk test. The data in C-D show mean ± SEM; F-O show mean ± SD. Statistical significance was determined by one-way ANOVA, followed by Tukey's multiple-comparisons test. *P<0.05; **P<0.01; ***P<0.001. Post-hoc power exceeded 80% for all comparisons. PVN, paraventricular nucleus; MI, myocardial infarction; V1a, Vasopressin 1a; GAR, $GABA_A$ receptor; NTS, nucleus tractus solitarii; LVEDD, left ventricular end-diastolic diameter; LVESD, lower left ventricular end-systolic diameter; LVEF, left ventricular ejection fraction; LVFS, left ventricular fraction shortening; SST, isomatostatin; CCK, cholecystokinin; VIP, vasoactive intestinal peptide; GLP-1, glucagon-like peptide 1.

vs. 7.74±0.24 mm, P<0.001; Fig. 2G), left ventricular ejection fraction (LVEF; 62.7±3.0% vs. 51.0±3.2%, P<0.01; Fig. 2H), left ventricular fraction shortening (LVFS; 38.3±1.5% vs. 26.4±2.1%, P<0.001; Fig. 2I) compared with the MI group. Compared with MI model rats, MI model rats that received apelin-13 continuous infusion into the PVN presented higher serum levels of SST (131.7±6.6 vs. 79.8±4.5 pg/ml; P<0.001), CCK (52.7±5.6 vs. 25.6±1.1 pg/100 ml; P<0.001), VIP (163.8±8.3 vs. 105.6±6.3 pg/ml; P<0.001) and GLP-1 (12.4±0.7 vs. 10.0±1.1 pg/ml; P<0.05; Fig. 2J-M), while showing markedly lower noradrenaline levels (578.3±51.5 vs. 825.0±89.4 pg/ml, P<0.001; Fig. 2N) and vasopressin levels (8.4±0.6 vs. 11.5±0.8 pg/ml, P<0.001; Fig. 2O). These findings suggested apelin-13 in the PVN improved post-MI cardiac function by activating both the vasopressinergic signaling and parasympathetic neuroendocrine pathways.

Effects of continuous apelin-13 infusion into the PVN on myocardial ischemia-associated apoptotic and inflammatory protein expression in MI rats. To investigate the cardioprotective mechanisms of PVN apelin-13 infusion, myocardial expression of ischemia-associated apoptotic and inflammatory proteins was analyzed by immunohistochemistry and multiplex fluorescent immunohistochemistry staining in heart tissues. Results from dual staining consistently demonstrated the involvement of both TGF-β/Smad and Bax/Bcl-2 signaling pathway in apelin-13-induced cardioprotection within the PVN. Post-MI rats showed a significant increase in TGF-β1 and Smad2 expression in heart tissue, which contributed to ventricular remodeling. PVN infusion of apelin-13 effectively suppressed these increases compared to untreated MI rats (Fig. 3A, B and E). Compared to sham-operated controls, post-MI rats exhibited markedly elevated Bax and reduced Bcl-2 expression in the myocardium. Notably, PVN administration of apelin-13 effectively reversed these alterations by downregulating Bax while upregulating Bcl-2 (Fig. 3C-E).

Comparison of AAV2-apelin-13 gene transfer vs. apelin-13 infusion in PVN effects on myocardial ischemia-related apoptotic and inflammatory proteins in MI model rats. MI models were established one day after implanting osmotic mini-pumps with apelin-13 or performing AAV2-apelin-13 gene transfer into PVN. Heart and brain tissues were collected at 3-, 7-, 14- and 28-days post-MI (Fig. 4Aa). First, successful microinjection of AAV2-apelin-13 gene into the PVN and its subsequent overexpression was confirmed (Fig. 4Ab-g). Subsequently, the effects of AAV2-apelin-13 gene transfer compared with continuous apelin-13 infusion in the PVN were compared. AAV2-apelin-13 gene transfer and continuous exogenous apelin-13 infusion into the PVN of MI model rats both induced time-dependent upregulation of Bcl-2 and downregulation of Bax in cardiac tissue (Fig. 4B-D). Concurrently, the expression of TGF-β1 and Smad2 progressively decreased over time (Fig. 4B, E and F). Correspondingly, V1a receptor expression in the PVN and NTS were elevated, while GARγ2 expression in the NTS declined gradually (Fig. 4B and G-I). At the same selected time points, there were no significant differences in the aforementioned protein expression between AAV2-apelin-13 gene transfer and continuous exogenous apelin-13 infusion. Therefore, subsequent studies will employ a combined approach using AAV2-mediated apelin-13 gene transfer specifically targeting the PVN, coupled with concurrent implantation of osmotic mini-pumps to deliver various antagonists to either the PVN or NTS for comprehensive study.

Effects of the APJ receptor and the GARγ2 receptor on the V1a receptor in primary cultured neurons. Prior to proceeding to further animal studies, it was assessed whether the APJ receptor and GARγ2 modulated V1a receptor expression in primary neuronal cultures. Immunofluorescence staining of primary culture neurons (Fig. 5A and B) revealed a time-dependent decrease in V1a receptor expression at both the protein (Fig. 5C and D) and mRNA levels (Fig. 5E) after treatment with either the APJ receptor antagonist F13A or the GAR agonist muscimol. Therefore, based on these observations, it was concluded that both APJ receptor antagonist and GAR agonist muscimol markedly altered V1a receptor expression, although the underlying mechanisms require further investigation.

The effect of apelin-13 overexpression (AAV2-apelin-13 gene transfer) in the PVN on V1a receptor-mediated improvement in the cardiac function in MI model rats. To investigate PVN V1a receptor-mediated cardioprotection, three interventions were employed: i) PVN AAV2-apelin-13 with PVN osmotic minipump delivering V1a antagonist SR49059; ii) PVN AAV2-apelin-13 with ipsilateral NTS minipump (SR49059); and iii) PVN AAV2-apelin-13 with ipsilateral NTS minipump containing the GAR agonist muscimol. The MI model was constructed one day after the transfer of the apelin-13 gene into PVN and the implantation of mini-pump (Fig. 6A). Prior to formal experiments, the AAV2-GFP group was compared with the sham-operated group and no significant difference was observed in relevant protein expression. Therefore, in this experiment, only the sham-operated group was used as controls (Fig. S1). The overexpression of apelin-13 in the PVN of the MI model rats markedly improved cardiac function, including the LVEF (79.1±1.8% vs. 66.2±2.2%; P<0.05; Fig. 6B), LVFS (45.0±1.9% vs. 32.8±1.3%; P<0.05; Fig. 6C), LVEDD (7.14±0.45 vs. 8.34±0.36 mm; P<0.05; Fig. 6D) and LVESD (5.01±0.17 vs. 6.12±0.23 mm; P<0.05) (Fig. 6E). These effects were attenuated by continuous PVN/NTS microinjection of the V1a antagonist SR49059 and continuous NTS microinjection of the GAR agonist muscimol (Fig. 6B-E). Compared with the continuous microinjection of SR49059 into the PVN in MI model rats overexpressing apelin-13, the continuous microinjection of SR49059 or muscimol into the NTS had fewer attenuating effects (Fig. 6B-E). The protective effects of apelin-13 overexpression were evident in Masson staining (Fig. 6F), TUNEL assay (Fig. 6G) and TTC staining (Fig. 6H) following microinjection of SR49059 into the PVN or NTS, or muscimol into the NTS. Bar graphs of the Masson, TUNEL and TTC staining results indicated that apelin-13 overexpression in the PVN markedly decreased fibrosis (29.0±3.4% vs. 56.0±3.4%; P<0.05; Fig. 6I), the mean fluorescence intensity (27.27±2.81 vs. 55.34±3.32 AU; P<0.05; Fig. 6J) and infarction area (24.4±4.1% vs. 46.8±4.9%; P<0.05; Fig. 6K). Compared with the microinjection of SR49059 into the PVN, the microinjection of SR49059 or muscimol into the NTS led to less fibrosis, a lower mean fluorescence intensity and a reduced infarction area (Fig. 6I-K). Compared with the

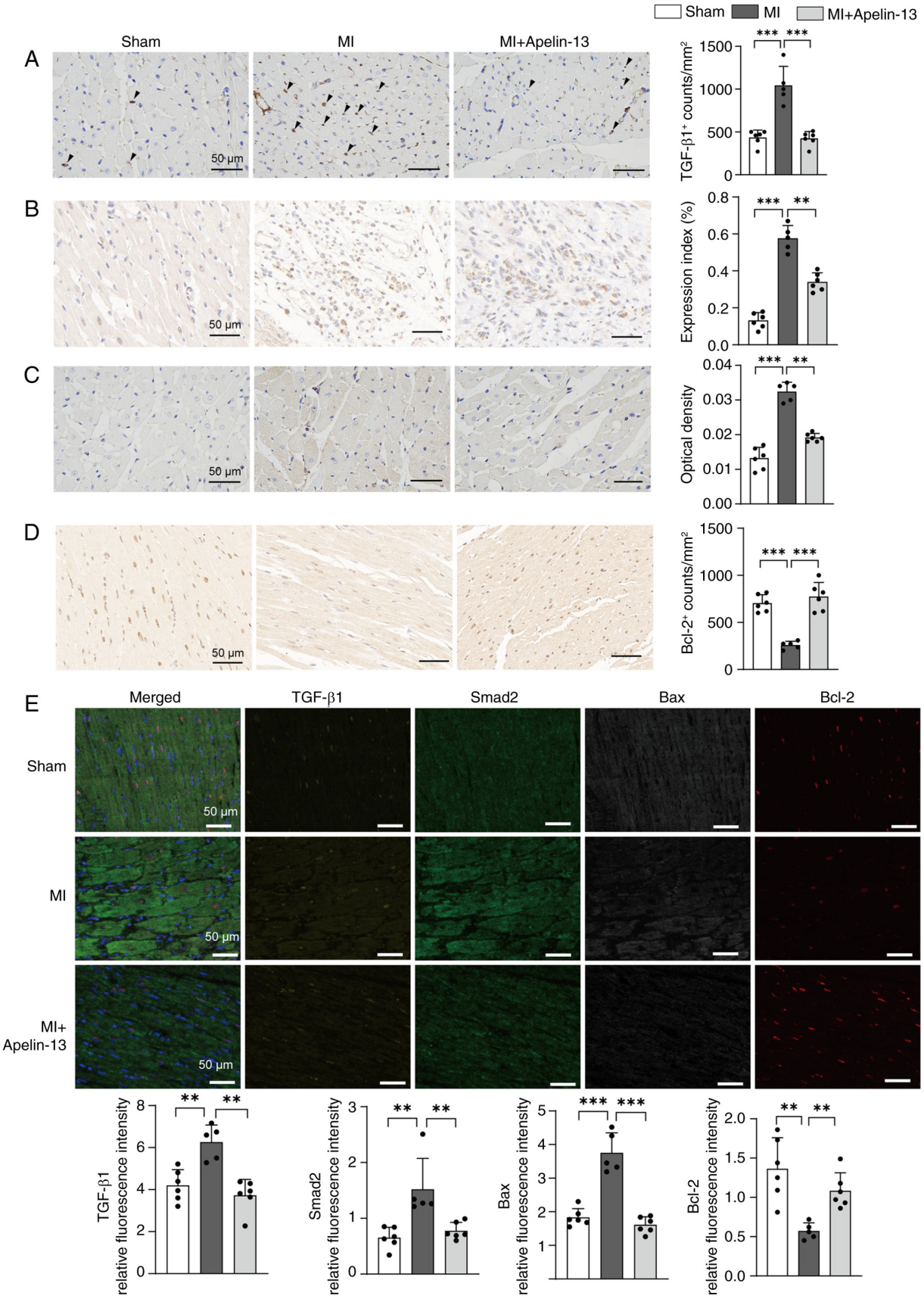

Figure 3. Effects of continuous apelin-13 infusion into the PVN on myocardial ischemia-associated apoptotic and inflammatory protein expression in MI rats. (A) Representative image and quantification of TGF-β1$^+$ cells. (B) Representative image and expression index of Smad2. (C) Representative image and optical density of Bax. (D) Representative image and quantification of Bcl-2$^+$ cells. (E) Representative multiplex fluorescent immunohistochemistry staining images and relative fluorescence intensity of TGF-β1, Smad2, Bax and Bcl-2 (n=6 in the sham-operated control group; n=5 in the MI group, one rat succumbed at 20 days; n=6 in the MI + apelin group). Normality was tested using the Shapiro-Wilk test. The data are shown as mean ± SD and were analyzed using one-way ANOVA, followed by Tukey's multiple-comparisons test. *P<0.05; **P<0.01; ***P<0.001. Post-hoc power exceeded 80% for all key comparisons. PVN, paraventricular nucleus; MI, myocardial infarction.

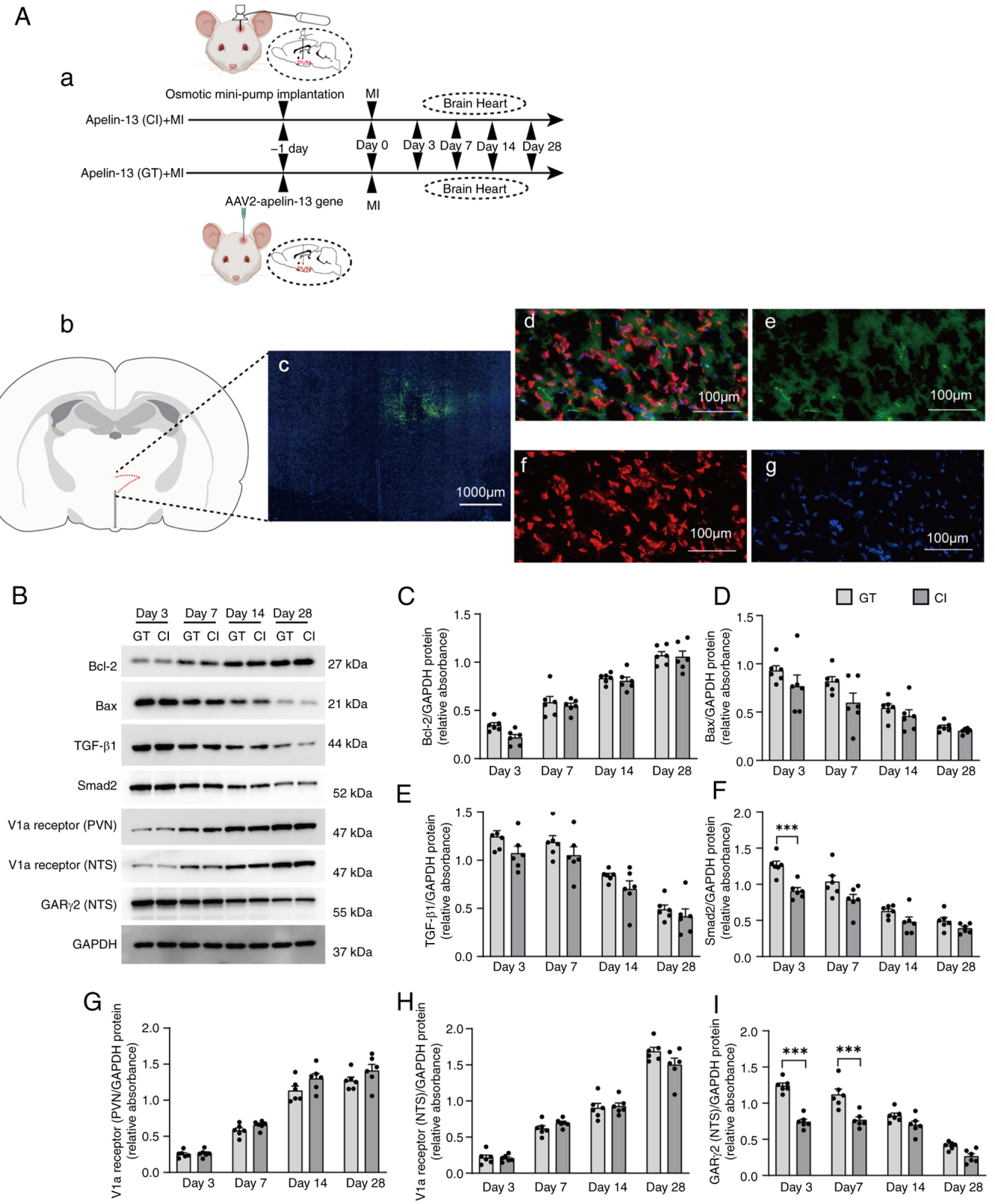

Figure 4. Comparison of effects between apelin-13 gene transfer and continuous infusion approaches. (Aa) After implanting apelin-13 osmotic mini-pumps or delivering AAV2-apelin-13 to the PVN, MI was induced and heart and brain tissues collected at 3-, 7-, 14- and 28-days post-MI (n=6 in each group). Location of the stained PVN brain sections shown in (b) and (c), based on the rat brain atlas of C. Watson and G. Paxinos (24). (c) Fluorescence micrograph (magnification, x10) demonstrating the localization of apelin-13 within the PVN. 3v is the third ventricle. (d) Overlap of (e), (f) and (g), showing that the green fluorescence is neuronally located. (e) Fluorescence micrograph (magnification, x40) indicating the localization of apelin-13 in PVN cells immunostained with an anti-apelin antibody (green). (f) Same field of cells as in panel (e), immunostained with anti-NeuN antibodies (red). (g) DAPI staining of the same field of cells in panel (e). (B) Molecular pathways regulating apoptotic and inflammatory pathways were assessed through western blotting of the expression of Bax, Bcl-2, TGF-β1 and Smad2 over time in MI model rats and the expression of the V1a receptor and GARγ2 induced by apelin-13 overexpression in the PVN. (C and I) Quantification of the fold change in target gene expression vs. GAPDH expression. The data (n=6 rats per group, 3 technical replicates) in (C-I) are shown as mean ± SEM and were analyzed via an unpaired two-tailed t test. *P<0.05; **P<0.01; ***P<0.001. Post-hoc power exceeded 80% for all key comparisons. PVN, paraventricular nucleus; MI, myocardial infarction; GT, gene transfer; CI, continuous infusion.

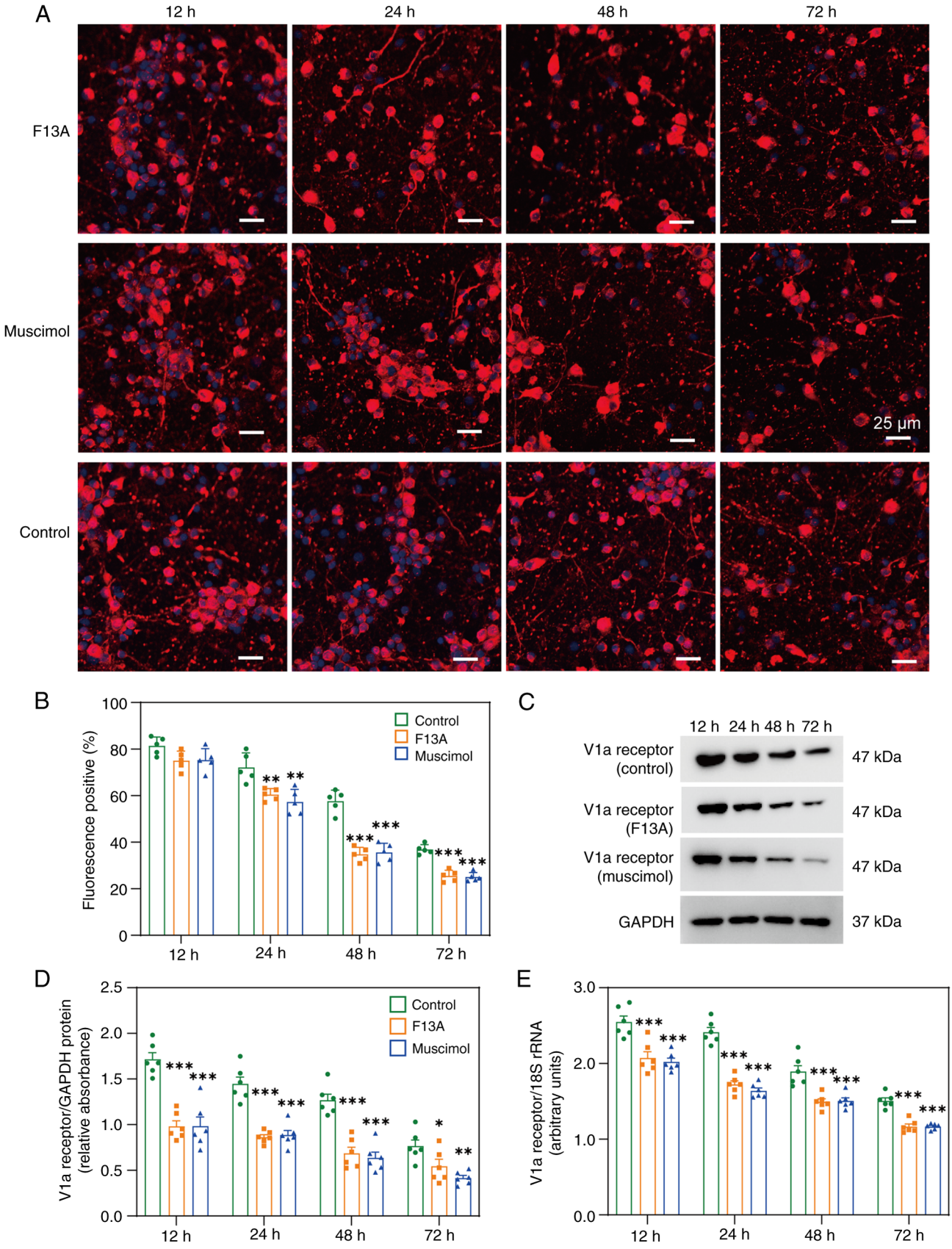

Figure 5. Effects of the APJ receptor and the GARγ2 receptor on the V1a receptor in primary cultured neurons. (A) Immunofluorescence of F13A-, muscimol- and control-treated primary neurons. Neurons were treated for 12, 24, 48, or 72 h. (B) Representative positive fluorescence. (C and D) Representative western blot image of the V1a receptor in primary cultured neurons treated with F13A and muscimol and quantification of V1a receptor expression. (E) mRNA expression levels of the V1a receptor in neurons treated with F13A and muscimol. The data (n=5 experiments) in (B) are shown as mean ± SD and were analyzed via one-way ANOVA, followed by Dunnett's multiple-comparisons test. Normality was tested using the Shapiro-Wilk test. The data (n=5; 3 technical replicates) in (D and E) are shown as mean ± SEM and were analyzed via one-way ANOVA, followed by Dunnett's multiple-comparisons test. *P<0.05; **P<0.01; and ***P<0.001vs. the control group. Post-hoc power exceeded 80% for all key comparisons. APJ, orphan G-protein-coupled; GAR, $GABA_A$ receptor; V1a, Vasopressin 1a.

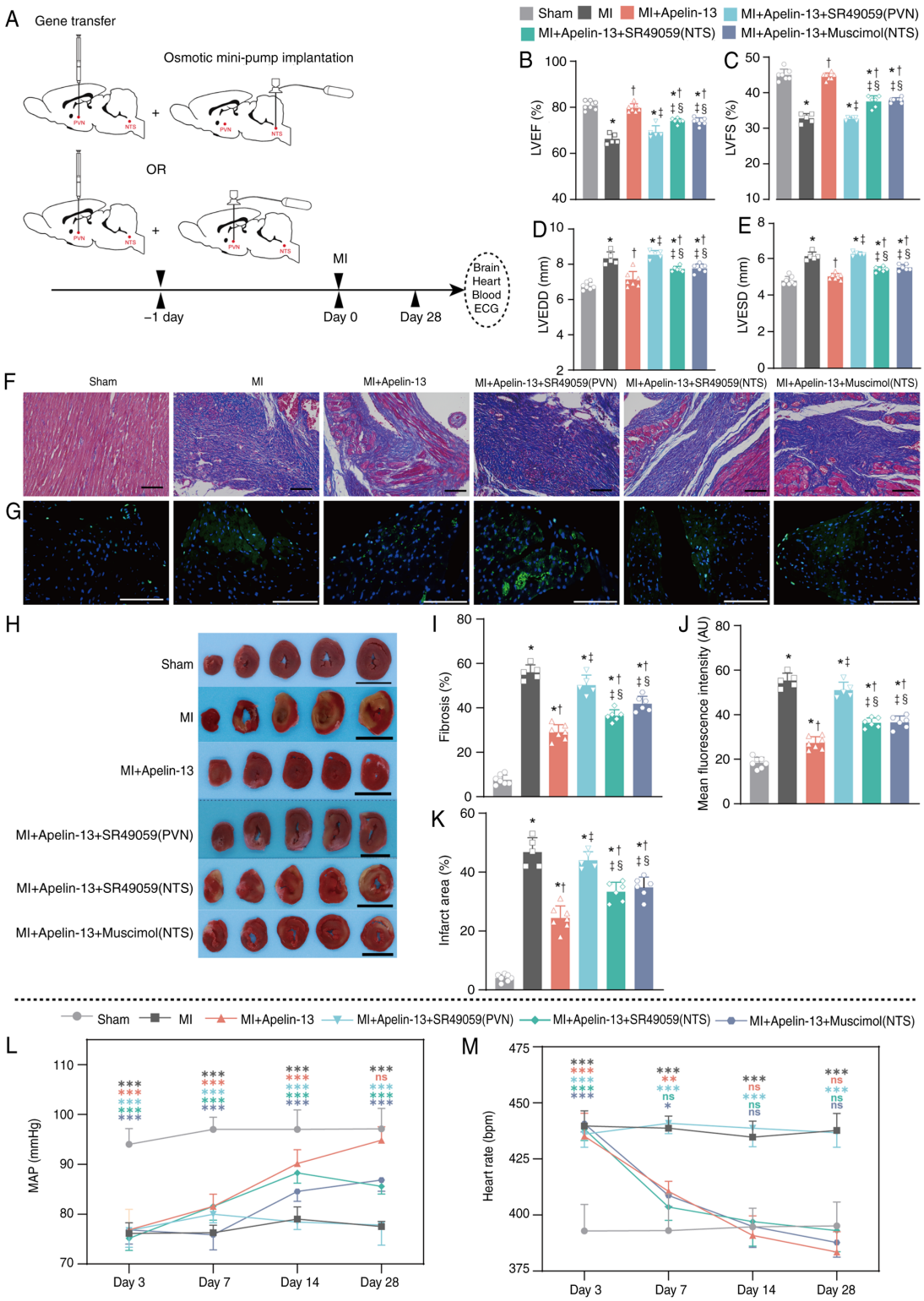

Figure 6. Effect of apelin-13 overexpression (AAV2-apelin-13 gene transfer) in the PVN on V1a receptor-mediated improvements in cardiac function and cardiac morphology in MI model rats. (A) The MI model was constructed one day following the transfer of the apelin-13 gene into PVN and the implantation of mini-pump (7 rats in each group). Echocardiographic results for (B) LVEF, (C) LVSF, (D) LVEDD and (E) LVESD. (F) Representative Masson's trichrome staining and (I) quantification. (G) Representative TUNEL staining and (J) quantification of TUNEL staining. (H) Representative TTC staining and (K) quantification. The black scale bar in F is 100 μm; the white scale bar in G is 50 μm; and the black scale bar in I is 1 cm. At 28 days after MI modelling, the sham-operated control group had 7 rats, the MI group had 5 rats (2 rats succumbed), the MI + apelin-13 group had 7 rats, the MI + apelin-13 + SR49059 (PVN) group had 5 rats (2 rats succumbed), the MI + apelin-13 + SR49059 (NTS) group had 6 rats (1 rat succumbed) and the MI + apelin-13 + muscimol (NTS) group had 6 rats (1 rat succumbed). Normality was tested using the Shapiro-Wilk test. The data in B-E and H-M are shown as means ± SDs and were analyzed using one-way ANOVA, followed by Tukey's multiple-comparisons test. In B-E and H-K, *P<0.05 vs. sham-operated control group; †P<0.05 vs. MI group; ‡P<0.05 vs. MI + apelin-13 group; §P<0.05 vs. MI + apelin-13 + SR49059(PVN); $^{\#}$P<0.05 vs. MI + apelin-13 + SR49059 (NTS). The (L) MAP and (M) heart rate were recorded in a conscious state at days 3, 7, 14 and 28 after MI modelling. *P<0.05; **P<0.01; ***P<0.001; and ns, not significant, vs. the sham-operated control group. Post-hoc power exceeded 80% for all key comparisons. PVN, paraventricular nucleus; V1a, Vasopressin 1a; MI, myocardial infarction; ECG, Echocardiographic; LVEF, left ventricular ejection fraction; LVFS, left ventricular fraction shortening; LVEDD, left ventricular end-diastolic diameter; LVESD, lower left ventricular end-systolic diameter; NTS, nucleus tractus solitarii; MAP, mean arterial pressure.

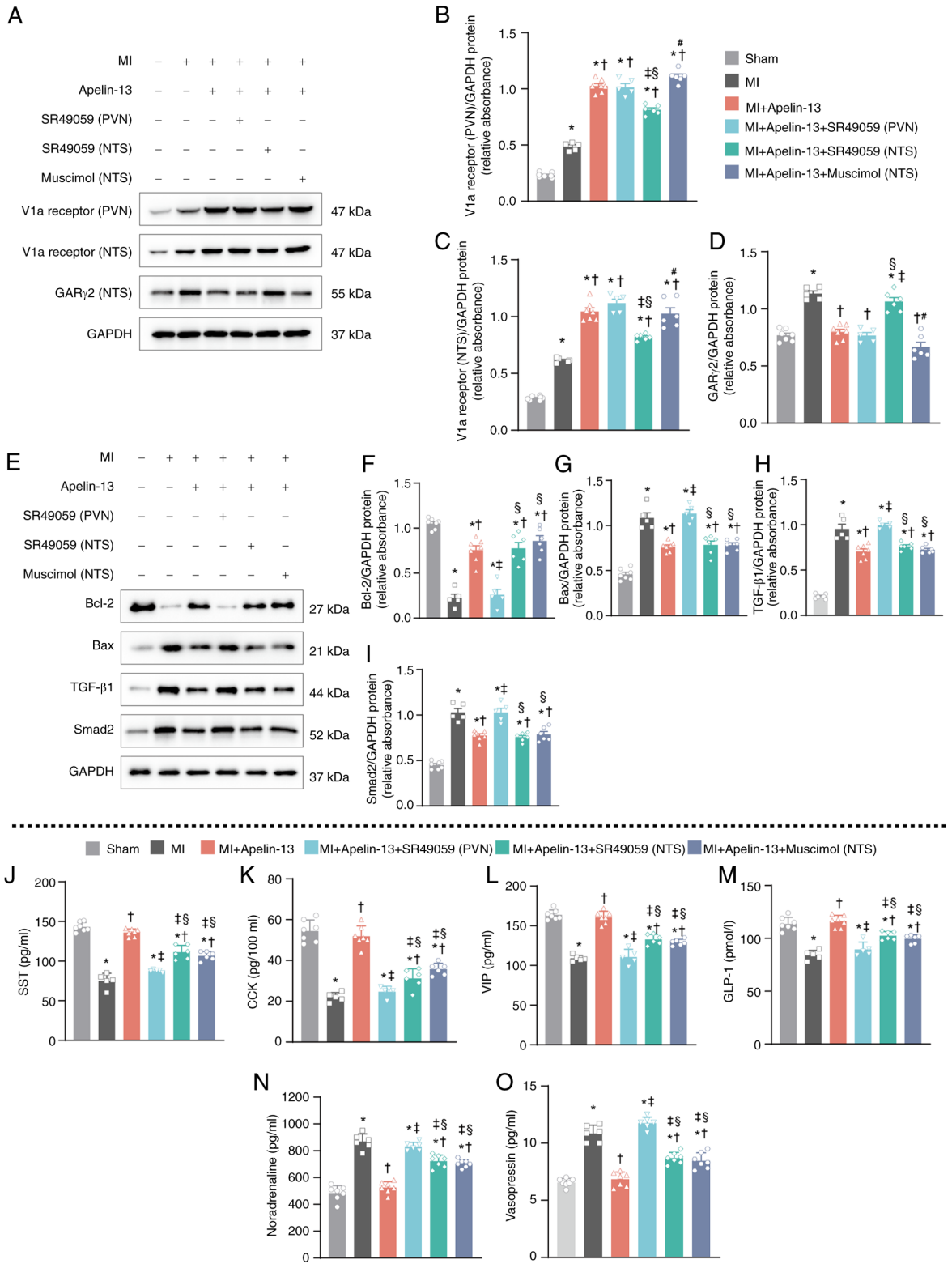

Figure 7. Mechanisms of the effect of apelin-13 overexpression (AAV2-apelin-13 gene transfer) in the PVN on V1a receptor-mediated improvement in cardiac function in MI model rats. (A) Representative western blot image of V1a receptor expression in the PVN or NTS and GARγ2 expression in the NTS. (B-D) Quantification of V1a receptor expression. (E) Representative western blotting to assess Bcl-2, Bax, TGF-β1 and Smad2 protein levels in the heart and (F-I) quantification of the protein levels. Plasma levels of (J) SST, (K) CCK, (L) VIP and (M) GLP-1 (n=7 in the sham-operated control group; n=5 in the MI group, 2 rats succumbed; n=7 in the MI + apelin-13 group; n=5 in the MI + apelin-13 + SR49059 (PVN) group, 2 rats succumbed; n=6 in the MI + apelin-13 + SR49059 (NTS) group, 1 rat succumbed; n=6 in the MI + apelin-13 + muscimol (NTS) group, 1 rat succumbed). Representative plasma levels of (N) noradrenaline and (O) vasopressin (n=7 in the sham-operated control group; n=6 in the MI group, 1 rat succumbed; n=7 in the MI + apelin-13 group; n=6 in the MI + apelin-13 + SR49059 (PVN) group, 1 rat succumbed; n=6 in the MI + apelin-13 + SR49059 (NTS) group, 1 rat succumbed; n=7 in the MI + apelin-13 + muscimol (NTS) group). Normality was tested using the Shapiro-Wilk test. The data in B-D and F-I show mean ± SEM; data in J-O are shown as mean ± SD and were analyzed via one-way ANOVA, followed by Tukey's multiple-comparisons test. In B-D and F-O, *P<0.05 vs. sham-operated control group; †P<0.05 vs. MI group; ‡P<0.05 vs. MI + apelin-13 group; §P<0.05 vs. MI + apelin-13 + SR49059 (PVN); #P<0.05 vs. MI + apelin-13 + SR49059 (NTS). Post-hoc power exceeded 80% for all key comparisons. PVN, paraventricular nucleus; V1a, Vasopressin 1a; MI, myocardial infarction; NTS, nucleus tractus solitarii; GAR, $GABA_A$ receptor; SST, isomatostatin; CCK, cholecystokinin; VIP, vasoactive intestinal peptide; GLP-1, glucagon-like peptide 1.

sham group, the MI rats with apelin-13 overexpression in the PVN had a similar MAP (94.9±2.7 vs. 97.1±4.1 mmHg; n=7; P>0.05) and HR (383.4±9.1 vs. 395.4±10.7 bpm; n=7; P>0.05; Fig. 6L and M) at 28 days after MI modelling. Continuous infusion of SR49059 into the PVN/NTS and muscimol into the NTS differentially affected the cardioprotective effects of apelin-13 in the PVN. The increase in V1a receptor expression in the PVN caused by AAV2-apelin-13 gene overexpression in the PVN was attenuated by the continuous microinjection of the V1a receptor antagonist SR49059 into the NTS but not into the PVN or the microinjection of the GAR antagonist muscimol into the NTS (Fig. 7A and B). In the NTS, increased V1a receptor expression caused by AAV2-apelin-13 gene overexpression in the PVN was not attenuated by the continuous microinjection of the V1a receptor antagonist SR49059 into the PVN or NTS or by the GAR antagonist muscimol into the NTS (Fig. 7A and C). The decrease in GARγ2 expression in the NTS caused by AAV2-mediated apelin-13 overexpression in the PVN was markedly attenuated by the continuous microinjection of the V1a receptor antagonist SR49059 in the NTS but not by the microinjection of SR49059 in the PVN or muscimol in the NTS (Fig. 7A and D). From the aforementioned results, it was found that the expression of both V1a receptors and GAR2 in the NTS was regulated by V1a receptors in the PVN. The apelin-13 gene overexpression-induced increase in Bcl-2 (Fig. 7E and F) and decrease in Bax (Fig. 7E and G), TGF-β1 (Fig. 7E and H) and Smad2 (Fig. 7E and I) were attenuated by the microinjection of SR49059 into the PVN but not into the NTS or by the microinjection of muscimol into the NTS. However, in the serum, the increased levels of SST (Fig. 7J), CCK (Fig. 7K), VIP (Fig. 7L) and GLP-1 (Fig. 7M) induced by apelin-13 overexpression in the PVN of the MI model rats were attenuated by the microinjection of SR49059 in the PVN or NTS and muscimol in the NTS. In contrast, the decreased level of noradrenaline (Fig. 7N) and vasopressin (Fig. 7O) increased after the microinjection of SR49059 in the PVN or NTS and muscimol in the NTS. Together, these findings demonstrated that the V1a receptor in the PVN/NTS and GARγ2 in NTS contribute to apelin-13-mediated cardioprotection in MI models through vasopressinergic signaling and PES.

Discussion

The present study provided novel evidence of the neural regulation of cardiac functions via apelin-13 in the PVN; apelin-13 upregulated the expression of the V1a receptor in the PVN and NTS and downregulated the expression of GARγ2 in the NTS. Effects of a V1a receptor antagonist and GARγ2 agonist further demonstrated that apelin-13 in the PVN is a novel factor involved in the centrally mediated neural control of myocardial injury, including in MI rat models. Furthermore, both myocardial TGF-β/Smad signaling and the Bax/Bcl-2 apoptotic balance contribute to the central-mediated cardioprotective effects of apelin-13 in PVN.

First, in MI model rats, apelin-13 expression was decreased in the PVN but not in the NTS or RVLM. The PVN is a critical central regulator of autonomic and humoral responses; it receives afferent inputs from visceral receptors and circulating hormones and then sends out projections to key cardiovascular brainstem centers and spinal cord preganglionic neurons, thereby modulating parasympathetic and sympathetic activity (27). The PVN is also involved in the treatment of MI-induced heart failure via the inhibition of oxidant signaling (6). Thus, it was hypothesized that there were more pathways involved in the mediation of cardiac function by apelin-13 in the PVN. Notably, V1a receptor expression in the PVN and NTS increased following apelin-13 microinjection into the PVN of MI model rats, whereas GARγ2 expression in the NTS decreased after apelin-13 microinjection; these findings were further confirmed in MI models with apelin-13 gene transmission. In the RVLM, the pressor effect evoked by the bilateral microinjection of apelin-13 as a modulating neurotransmitter in normotensive rats via the V1a receptor affects vascular tone independent of GAR, whereas the presence of presynaptic V1a receptors affects vasopressin release from the PVN-RVLM projecting fibers (15). The observations in the present study suggested that synaptic V1a receptors act as communicators between the PVN and NTS for apelin-13-mediated nerve connections and GARγ2 expression in the NTS.

These findings indicated that myocardial injury induced the downregulation of apelin-13 expression in the PVN and that upregulating apelin-13 expression in the PVN improved cardiac function. Thus, it was hypothesized that the apelin/APJ system is involved in the PVN-NTS axis for the regulation of cardiac function, a novel concept of heart-brain interactions. The heart and the brain are linked by multiple feedback signals and the concept of cardio-cerebral syndrome in heart failure has been built on the bidirectional interactions of failing heart and neuronal signals (28). A previous review indicated that the mechanisms of brain-heart interactions include the physiological effects of sympathetic and parasympathetic nerve activities, central pathways regulating autonomic outflow, reflex control of autonomic outflow and the integrative regulation of autonomic outflow to the heart (29). More specifically, the sympathetic and parasympathetic branches of the autonomic nervous system directly control the heart and parasympathetic postganglionic fibers innervate the atrial and ventricular myocardium by releasing acetylcholine and VIP (30). Consistently, in the present study, as a critical mediator of synaptic inhibition in the brain (31), the expression of the γ2 subunit of GAR in the NTS decreased after apelin-13 overexpression in the PVN, which indirectly elevated parasympathetic efferent excitability to activate the PES.

The V1a receptor is a transmembrane protein that belongs to the G protein-coupled receptor superfamily. The combined activation of V1a receptors by vasopressin in the PVN has been shown to increase renal sympathetic nerve activity (32). Subsequent to MI, within the PVN, a notable elevation in the expression level of the V1a receptor was observed. This augmented expression subsequently led to a significant enhancement in the modulation of the autonomic cardiovascular system, thereby playing a crucial role in the intricate physiological adjustments that occur in response to the myocardial damage. In NTS, V1a receptor can influence the transmission and integration of baroreceptor reflex signals, which play a crucial role in regulating blood pressure and heart rate. Dysfunction of the V1a receptor-mediated modulation in the NTS may contribute to abnormal blood pressure regulation and heart rate variability after MI. The present

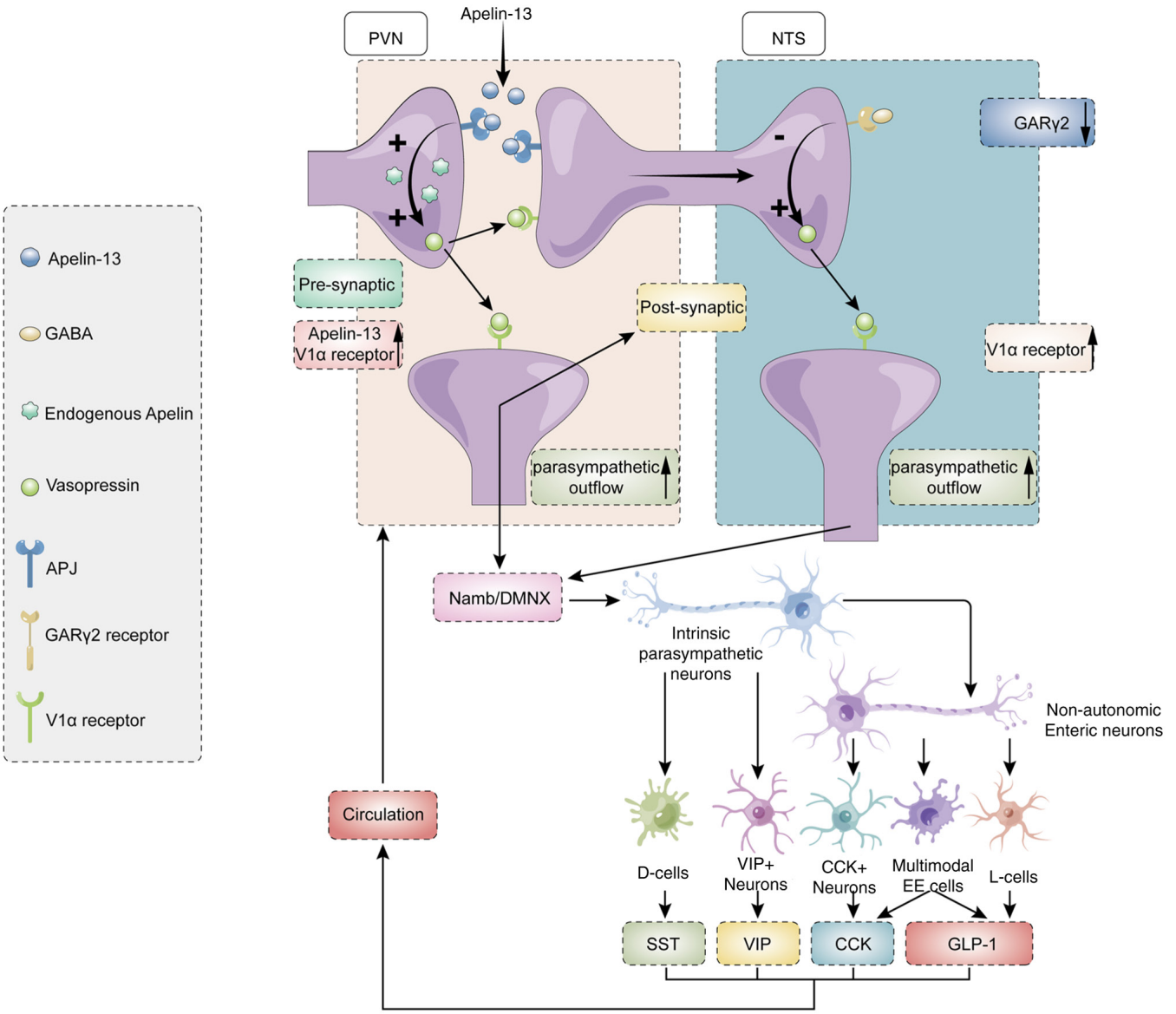

Figure 8. Graphical model summarizing the hypothesized pathway. Overexpression of apelin-13 in the PVN promotes upregulation of V1a receptors in both the PVN and NTS, while downregulating GARγ2 in the NTS. These neural modifications collectively enhance parasympathetic outflow. Furthermore, paraventricular endocrine system secretes circulating neurohumoral factors that systemically mediate cardioprotection. PVN, paraventricular nucleus; V1a, Vasopressin 1a; MI, myocardial infarction; NTS, nucleus tractus solitarii; GAR, $GABA_A$ receptor; SST, isomatostatin; CCK, cholecystokinin; GLP-1, glucagon-like peptide 1; VIP, vasoactive intestinal peptide.

study showed that apelin-13 overexpression in the PVN of MI model rats further elevated the increased V1a receptor expression in the PVN and NTS, indicating its involvement in apelin-13-mediated cardiac function.

The apelin/APJ system plays several important roles in the neurohormonal regulation of heart function, including vasodilatory effects, positive inotropic effects, fluid balance regulation, antiapoptotic effects and interactions with other neurohormonal systems (25,33). The present study revealed that the improved cardiac function mediated by apelin/APJ in the PVN involves PES activation by apelin-13 overexpression, including an increase in the expression of four effectors, namely, SST, CCK, GLP-1 and VIP. SST has been shown to exert a direct cardiocytoprotective effect against simulated cardiomyocyte injury via SST receptor 1 and SST receptor 2 in cardiomyocytes and vascular endothelial cells (34). CCK, GLP-1 and VIP are involved in cardiovascular regulation via different mechanisms in the circulation (35-37). Thus, it was hypothesized that the PES plays an important role in the heart-brain circuit. While the pro-fibrotic and remodeling role of TGF-β/Smad signaling in the heart has been well established (38), the histomorphometry and molecular analyses of the present study demonstrated that apelin-13 in the PVN mediates cardioprotection by modulating PES, ultimately downregulating the TGF-β/Smad signaling pathway, thereby attenuating cardiac fibrosis and remodeling. Meanwhile, the regulation of myocardial Bax/Bcl-2 expression was also involved in the central cardioprotective effects mediated by apelin-13 in the PVN.

The present study provided novel evidence that PVN-derived apelin-13 modulates cardiac function through dual mechanisms: Upregulating V1a receptor expression in

both PVN and NTS nuclei and downregulating GARγ2 expression specifically in the NTS. Mechanistically, PVN apelin-13 overexpression improved cardiac performance via V1a receptors (PVN/NTS) and GARγ2 (NTS)-dependent pathways. This regulation involves both parasympathetic signaling and myocardial ischemia-associated pro-apoptotic/pro-inflammatory cascades, establishing the first evidence for central neural control of cardiovascular pathogenesis (Fig. 8).

Despite these meaningful findings, the present study had certain limitations. Although it found novel evidence of neural control of cardiomyocyte injury, the mechanism of interaction between the PVN and NTS is not fully clear, except for direct exposure to the neurotransmitter apelin-13 and vasopressin. Importantly, the V1a receptor and GARγ2 in the NTS are indirectly regulated by the apelin/APJ system in the NTS, but postsynaptic GAR currents should be considered for modulating receptor expression. Therefore, other unclear mechanisms are involved in receptor interactions between the PVN and NTS. To address the limitation of lacking electrophysiological evidence, future work will directly record from PVN neurons that project to the NTS to determine how their firing activity changes following apelin-13 administration. Due to the technical challenges in precisely isolating the PVN and NTS from neonatal rats, primary neuronal culture studies cannot fully reflect the regulatory effects of APJ and GARγ2 on V1a receptor expression in these nuclei. Moreover, the interaction mechanisms between these receptors within specific nuclei require further investigation. The mechanism by which GARγ2 regulates V1a receptor expression remains unclear. Candidate transcription factors potentially mediating this regulation include nuclear factor-κB (NF-κB) (39,40), early growth response protein 1 (EGR1) (41,42) and cAMP response element-binding protein (CREB) (43,44). Subsequent studies should further investigate this mechanism through integrated approaches including electrophysiology and single-cell RNA-sequencing. Since drugs may diffuse from injection sites and transgene expression may spread beyond target areas, other hypothalamic regions might unexpectedly participate in cardiac regulation. Vasopressin present in the cerebrospinal fluid (CSF) can interact with the HPA axis. This interaction can enhance the release of adrenocorticotropic hormone from the anterior pituitary gland to modulate cardiac function (45). However, the levels of vasopressin in CSF were unfortunately not assessed. Finally, four peptides that act as neurotransmitters are released through a complex network of gut sensing and vagal mechanisms. Other neuropeptide levels could also be affected by apelin-13 in the PVN; however, these levels were not detected or explored in the present study. The present study selected male rats to minimize sex hormone variability and ensure precision in stereotaxic brain nucleus targeting during injections and minipump implantation. Consequently, findings may not generalize to females; subsequent studies will further validate results in ovariectomized and intact female models.

In conclusion, apelin-13 in the PVN performs neural control for cardiac function via the V1a receptor in the PVN and NTS and GARγ2 in the NTS, offering novel evidence of brain-heart interactions. The present study provided evidence for improving cardiac function through the CNS in the future.

Acknowledgements

Not applicable.

Funding

The present study was supported by the National Natural Science Foundation of China (grant no. 82070361).

Availability of data and materials

The data generated in the present study may be found in the Sequence Read Archive under at the following URL: https://www.ncbi.nlm.nih.gov/gene?cmd=Search&doptcmdl=EntrezGene&term=58812, https://www.ncbi.nlm.nih.gov/gene/2550, https://www.ncbi.nlm.nih.gov/gene/552 and https://www.ncbi.nlm.nih.gov/gene/2566.

Authors' contributions

WY, DW and XZ conducted the experiments. CX and WY designed the experiments and analyzed the data. DW and CX drafted the manuscript and all authors edited the manuscript. WY and DW confirmed the authenticity of all the raw data. All authors read and approved the final manuscript.

Ethics approval and consent to participate

Not applicable.

Patient consent for publication

Not applicable.

Competing interests

The authors declare that they have no competing interests.

References

1. Chen Z, Venkat P, Seyfried D, Chopp M, Yan T and Chen J: Brain-heart interaction: Cardiac complications after stroke. Circ Res 121: 451-468, 2017.
2. Simats A, Sager H and Liesz A: Heart brain axis in health and disease: Role of innate and adaptive immunity. Cardiovasc Res 120: 2325-2335, 2025.
3. Zhao B, Li T, Fan Z, Yang Y, Shu J, Yang X, Wang X, Luo T, Tang J, Xiong D, *et al*: Heart-brain connections: Phenotypic and genetic insights from magnetic resonance images. Science 380: abn6598, 2023.
4. Herman JP and Tasker JG: Paraventricular hypothalamic mechanisms of chronic stress adaptation. Front Endocrinol (Lausanne) 7: 137, 2016.
5. Benarroch EE: The central autonomic network: Functional organization, dysfunction, and perspective. Mayo Clin Proc 68: 988-1001, 1993.
6. Infanger DW, Cao X, Butler SD, Burmeister MA, Zhou Y, Stupinski JA, Sharma RV and Davisson RL: Silencing nox4 in the paraventricular nucleus improves myocardial infarction-induced cardiac dysfunction by attenuating sympathoexcitation and peri-infarct apoptosis. Circ Res 106: 1763-1774, 2010.
7. Tatemoto K, Hosoya M, Habata Y, Fujii R, Kakegawa T, Zou MX, Kawamata Y, Fukusumi S, Hinuma S, Kitada C, *et al*: Isolation and characterization of a novel endogenous peptide ligand for the human APJ receptor. Biochem Biophys Res Commun 251: 471-476, 1998.

8. Lee DK, Cheng R, Nguyen T, Fan T, Kariyawasam AP, Liu Y, Osmond DH, George SR and O'Dowd BF: Characterization of apelin, the ligand for the APJ receptor. J Neurochem 74: 34-41, 2000.
9. Yang N, Li T, Cheng J, Tuo Q and Shen J: Role of apelin/APJ system in hypothalamic-pituitary axis. Clin Chim Acta 499: 149-153, 2019.
10. Lv SY, Chen WD and Wang YD: The apelin/APJ system in psychosis and neuropathy. Front Pharmacol 11: 320, 2020.
11. Masaki T, Yasuda T and Yoshimatsu H: Apelin-13 microinjection into the paraventricular nucleus increased sympathetic nerve activity innervating brown adipose tissue in rats. Brain Res Bull 87: 540-543, 2012.
12. Ji M, Wang Q, Zhao Y, Shi L, Zhou Z and Li Y: Targeting hypertension: superoxide anions are involved in apelin induced long-term high blood pressure and sympathetic activity in the paraventricular nucleus. Curr Neurovasc Res 16: 455-464, 2019.
13. Zhang Q, Yao F, Raizada MK, O'Rourke ST and Sun C: Apelin gene transfer into the rostral ventrolateral medulla induces chronic blood pressure elevation in normotensive rats. Circ Res 104: 1421-1428, 2009.
14. De Mota N, Reaux-Le Goazigo A, El Messari S, Chartrel N, Roesch D, Dujardin C, Kordon C, Vaudry H, Moos F and Llorens-Cortes C: Apelin, a potent diuretic neuropeptide counteracting vasopressin actions through inhibition of vasopressin neuron activity and vasopressin release. Proc Natl Acad Sci USA 101: 10464-10469, 2004.
15. Griffiths PR, Lolait SJ, Harris LE, Paton JFR and O'Carroll AM: Vasopressin V1a receptors mediate the hypertensive effects of [Pyr1]apelin-13 in the rat rostral ventrolateral medulla. J Physiol 595: 3303-3318, 2017.
16. Czarzasta K, Cudnoch-Jedrzejewska A, Szczepanska-Sadowska, Fus L, Puchalska L, Gondek A, Dobruch J, Gomolka R, Wrzesien R, Zera T, *et al*: The role of apelin in central cardiovascular regulation in rats with post-infarct heart failure maintained on a normal fat or high fat diet. Clin Exp Pharmacol Physiol 43: 983-994, 2016.
17. Kuriyama K, Hirouchi M and Kimura H: Neurochemical and molecular pharmacological aspects of the GABA(B) receptor. Neurochem Res 25: 1233-1239, 2000.
18. Li B, Liu Q, Xuan C, Guo L, Shi R, Zhang Q, O'Rourke ST, Liu K and Sun C: GABAB receptor gene transfer into the nucleus tractus solitarii induces chronic blood pressure elevation in normotensive rats. Circ J 77: 2558-2566, 2013.
19. Dampney RA: Functional organization of central pathways regulating the cardiovascular system. Physiol Rev 74: 323-364, 1994.
20. Korpal AK, Han SY, Schwenke DO and Brown CH: A switch from GABA inhibition to excitation of vasopressin neurons exacerbates the development angiotensin II-dependent hypertension. J Neuroendocrinol: Dec 9, 2017 (Epub ahead of print).
21. Klok MD, Jakobsdottir S and Drent ML: The role of leptin and ghrelin in the regulation of food intake and body weight in humans: A review. Obes Rev 8: 21-34, 2007.
22. Gorky J and Schwaber J: Conceptualization of a parasympathetic endocrine system. Front Neurosci 13: 1008, 2019.
23. Livak KJ and Schmittgen TD: Analysis of relative gene expression data using real-time quantitative PCR and the 2(-Delta Delta C(T)) method. Methods 25: 402-408, 2001.
24. Watson C and Paxinos G: The rat brain in stereotaxic coordinates, 5th ed. Amsterdam: Elsevier, 2004, pp. 51-57.
25. Zhao Y, Li Y, Li Z, Xu B, Chen P and Yang X: Superoxide anions modulate the performance of apelin in the paraventricular nucleus on sympathetic activity and blood pressure in spontaneously hypertensive rats. Peptides 121: 170051, 2019.
26. Kc P, Balan KV, Tjoe SS, Martin RJ, Lamanna JC, Haxhiu MA and Dick TE: Increased vasopressin transmission from the paraventricular nucleus to the rostral medulla augments cardiorespiratory outflow in chronic intermittent hypoxia-conditioned rats. J Physiol 588: 725-740, 2010.
27. Benarroch EE: Paraventricular nucleus, stress response, and cardiovascular disease. Clin Auton Res 15: 254-263, 2005.
28. Havakuk O, King KS, Grazette L, Yoon AJ, Fong M, Bregman N, Elkayam U and Kloner RA: Heart failure-induced brain injury. J Am Coll Cardiol 69: 1609-1616, 2017.
29. Silvani A, Calandra-Buonaura G, Dampney RA and Cortelli P: Brain-heart interactions: Physiology and clinical implications. Philos Trans A Math Phys Eng Sci 374: 20150181, 2016.
30. Coote JH: Myths and realities of the cardiac vagus. J Physiol 591: 4073-4085, 2013.
31. Kim JJ and Hibbs RE: Direct structural insights into GABAA receptor pharmacology. Trends Biochem Sci 46: 502-517, 2021.
32. Komnenov D, Quaal H and Rossi NF: V1a and V1b vasopressin receptors within the paraventricular nucleus contribute to hypertension in male rats exposed to chronic mild unpredictable stress. Am J Physiol Regul Integr Comp Physiol 320: R213-R225, 2021.
33. Dalzell JR, Rocchiccioli JP, Weir RA, Jackson CE, Padmanabhan N, Gardner RS, Petrie MC and McMurray JJ.: The emerging potential of the apelin-APJ system in heart failure. J Card Fail 21: 489-498, 2015.
34. Vörös I, Sághy É, Pohóczky K, Makkos A, Onódi Z, Brenner GB, Baranyai T, Ágg B, Váradi B, Kemény Á, *et al*: Somatostatin and its receptors in myocardial ischemia/reperfusion injury and cardioprotection. Front Pharmacol 12: 663655, 2021.
35. Han Z, Bi S, Xu Y, Dong X, Mei L, Lin H and Li X: Cholecystokinin expression in the development of myocardial hypertrophy. Scanning 2021: 8231559, 2021.
36. Simms-Williams N, Treves N, Yin H, Lu S, Yu O, Pradhan R, Renoux C, Suissa S and Azoulay L: Effect of combination treatment with glucagon-like peptide-1 receptor agonists and sodium-glucose cotransporter-2 inhibitors on incidence of cardiovascular and serious renal events: Population based cohort study. BMJ 385: e078242, 2024.
37. Duggan KA, Hodge G, Chen J and Hunter T: Vasoactive intestinal peptide infusion reverses existing myocardial fibrosis in the rat. Eur J Pharmacol 862: 172629, 2019.
38. Sarker M, Chowdhury N, Bristy AT, Emran T, Karim R, Ahmed R, Shaki MM, Sharkar SM, Sayedur Rahman GM and Reza HM: Astaxanthin protects fludrocortisone acetate-induced cardiac injury by attenuating oxidative stress, fibrosis, and inflammation through TGF-β/Smad signaling pathway. Biomed Pharmacother 181: 117703, 2024.
39. Liu H, Yu L, Yang L and Green MS: Vasoplegic syndrome: An update on perioperative considerations. J Clin Anesth 40: 63-71, 2017.
40. Fu Q, Yu Q, Luo H, Liu Z, Ma X, Wang H and Cheng Z: Protective effects of wogonin in the treatment of central nervous system and degenerative diseases. Brain Res Bull 221: 111202, 2025.
41. Liu Y, Donovan M, Jia X and Wang Z: The ventromedial hypothalamic circuitry and male alloparental behaviour in a socially monogamous rodent species. Eur J Neurosci 50: 3689-3701, 2019.
42. Loveland JL and Fernald RD: Differential activation of vasotocin neurons in contexts that elicit aggression and courtship. Behav Brain Res 317: 188-203, 2017.
43. Yan R, Liu Q, Zhang D, Li K, Li Y, Nie Y, Zhang Y, Li P, Mao S and Li H: Inhibition of spreading depolarizations by targeting GABAA receptors and voltage-gated sodium channels improves neurological deficits in rats with traumatic brain injury. Br J Pharmacol: Jun 24, 2025 (Epub ahead of print).
44. Greenwood M, Gillard BT, Murphy D and Greenwood MP: Dimerization of hub protein DYNLL1 and bZIP transcription factor CREB3L1 enhances transcriptional activation of CREB3L1 target genes like arginine vasopressin. Peptides 179: 171269, 2024.
45. Szczepanska-Sadowska E, Czarzasta K, Bogacki-Rychlik W and Kowara M: The interaction of vasopressin with hormones of the hypothalamo-pituitary-adrenal axis: The significance for therapeutic strategies in cardiovascular and metabolic diseases. Int J Mol Sci 25: 7394, 2024.